https://doi.org/10.5194/essd-2025-727
Preprint. Discussion started: 16 January 2026

Open Access Earth System Science Data Discussions

The OCEAN ICE hydrography profiles compilation and climatology

Shenjie Zhou[1], Pierre Dutrieux[1], Claudia Giulivi[2], Andrew Meijers[1], Won Sang Lee[3], Tae-Wan Kim[3], Tore Hattermann[4], Markus Janout[5]

[1]British Antarctic Survey, Cambridge, UK
[2]Lamont-Doherty Earth Observatory, Columbia University, Palisades, USA
[3]Korea Polar Research Institute, Incheon, South Korea
[4]Norwegian Polar Institute, Tromsø, Norway
[5]Alfred Wegener Institute for Polar and Marine Research, Bremerhaven, Germany

Correspondence to: Shenjie Zhou (shezhou@bas.ac.uk)

Abstract. A compilation of in situ temperature and salinity profiles south of 45°S is assembled, drawing from multiple data centers and sensor sources. This database is then used to create a new Southern Ocean climatology, adopting an interpolation scheme that takes into account ocean depth and mean ocean dynamics, influenced by methods developed for the Southern Ocean Atlas. This interpolation scheme is designed to consider along flow spatial coherency and the distinct dynamic regimes between Antarctic shelf seas and the Southern Ocean. Initial exploration of the profile compilation investigates the type of variability timescales one could reasonably start to analyze in different sectors around Antarctica. A comparison between the climatology product and the World Ocean Atlas climatology, the most used product to date, indicates that the OCEAN ICE climatology provides significant improvements in Antarctic shelf seas, including a more detailed representation of the unique water masses they host. The profile compilation is available in NetCDF format with the SEANOE database at https://doi.org/10.17882/99787, and the climatology product is available at https://doi.org/10.17882/103946. Both the hydrography profiles compilation and the hydrography climatology products are generated under the endorsement of Ocean-Cryosphere Exchanges in ANtarctica: Impacts on Climate and the Earth System (OCEAN ICE) project (https://ocean-ice.eu/) funded by the European Commission and UK Research and Innovation.

1 Introduction

The concept of World Ocean Circulation Experiment (WOCE) originated in the 1970s, and by early 2000s provided the first global view of Conductivity-Temperature-Depth (CTD) distribution for the world oceans (Siedler et al., 2001). Since then regular full depth hydrographic sections have been repeated using research vessels to obtain quasi-decadal in situ snapshots of ocean temperature and salinity (Fig. 1b). This approach provided a fairly sparse but evenly distributed CTD dataset across the Southern Ocean and facilitated the creation of the Southern Ocean Data Base (SODB) and its associated climatology product (Fig. 1a, Orsi and Whitworth 2005). The full-depth measurements also allowed basin-wide examination of deep water mass properties, full-depth ocean heat content and their variability (Johnson et al. 2024), identifying a large scale

https://doi.org/10.5194/essd-2025-727
Preprint. Discussion started: 16 January 2026

multi-decadal warming and contraction trend in the Antarctic Bottom Water (AABW) (Purkey and Johnson 2010, 2012, 2013; Johnson and Purkey 2024). AABW is a climatically-critical water mass originating from Antarctic coastal seas that ventilates the abyssal ocean and sequesters heat and carbon into the deep ocean through sea ice formation within coastal polynyas (Tamura et al. 2016, Zhou et al. 2023).

Since the early 21st century, the advent of Argo float profilers and instrumented seals have both significantly increased the spatial coverage of the data sampling in the Southern Ocean and efforts to produce state of the art ocean climatology have been continuous through rounds of data incorporation into the World Ocean Atlas. These three data sources (ship-based CTD, Argo floats and instrumented-seal data) nicely compensate each other in terms of spatial and temporal coverage. Notably, the seal data has largely enhanced the sampling over Antarctic continental shelf seas that research vessels and Argo float profilers have historically struggled to reach on a regular basis or cover extensively (Fig. 2b, 2c and 2e), while Argo float profilers provided much needed coverage north of the Antarctic continental shelf break (Fig. 2b and 2e). Ship-based CTD casts have a necessarily smaller spatial footprint, and a summer-oriented sampling bias, occasionally reaching the deep South on Antarctic continental shelves (Fig. 2d, 2e and 2g), but importantly extend *in-situ* measurements back to the 1970s, whilst Argo float profilers and instrumented-seal measurements only started to be deployed post 2000 (Fig. 2f). The addition of Argo floats and instrumented-seal measurements reduces the seasonal bias inherent to ship-based CTD measurements (Fig. 2g).

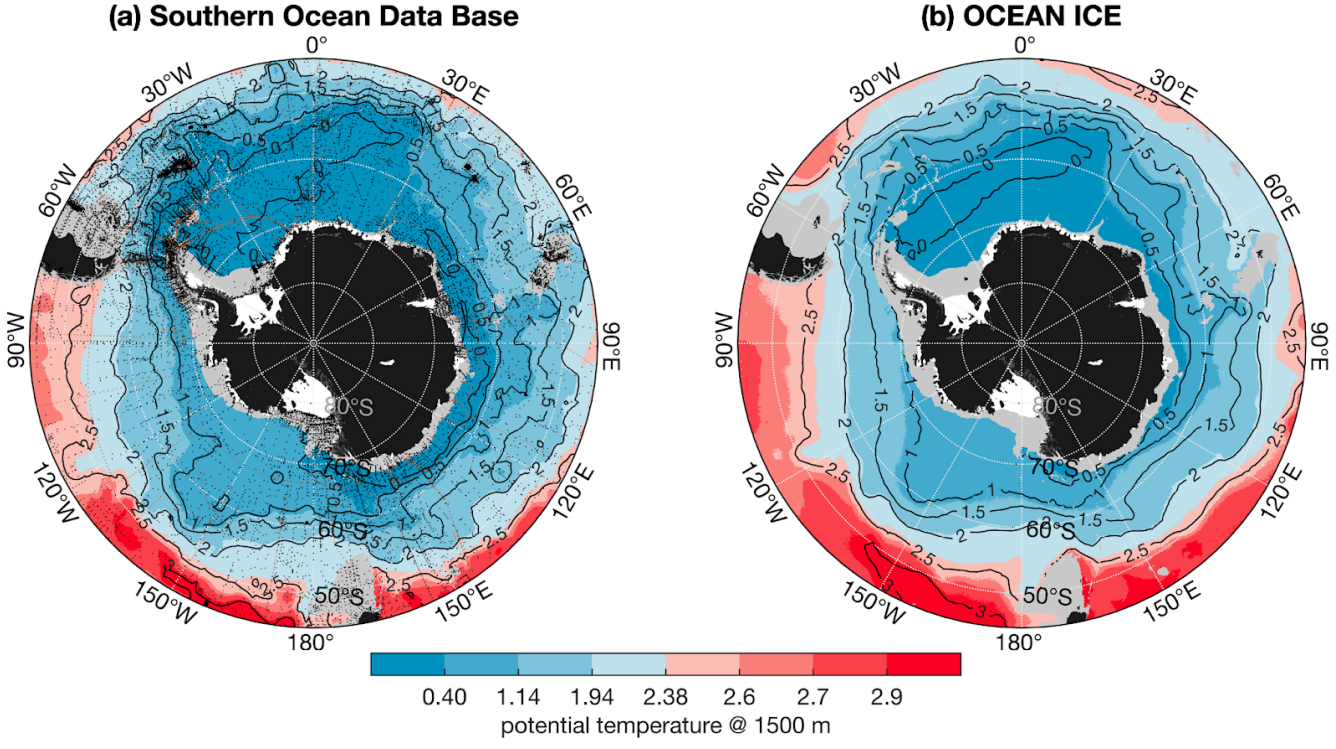

https://doi.org/10.5194/essd-2025-727
Preprint. Discussion started: 16 January 2026

Figure 1. (a) Locations of stations (black dots) of data used in the SODB laying on top of the colourshades (and labeled contours) depicting 1500m potential temperature field using gridded SODB climatology (reproduced from Orsi and Whitworth 2005). , Black and orange dots are scattered CTD stations and WOCE CTD transects. Station data is available at https://zenodo.org/records/4071923. Gridded SODB product for the potential temperature map at 1500m is available at https://woceatlas.tamu.edu/atlas/printed/SOA_1500m.txt. Note that the gridded data available is organized in vector format, therefore the map shown here is a result of the SODB 1500 m potential temperature re-interpolated onto a 10km resolution polar stereographic grid. (b) potential temperature at 1500 m from the new OCEAN ICE (O:I) climatology.

The Southern Ocean stands as a key regulator of the climate systems due to its disproportionate importance in sequestering excess heat and carbon from the atmosphere (Frölicher et al., 2015, Williams et al. 2024) mainly due to the broad, quasi-circum-Antarctic spreading of the upwelling and subduction of cold and carbon depleted deep water mass within the Antarctic Circumpolar Current. The freshwater input from the Antarctic ice mass loss modulates the upper ocean stratification which is in turn key to the upwelling processes and deep coastal and open ocean convection (Sallée et al. 2023). Furthermore, ocean-driven melting of Antarctic ice shelves reduces their buttressing effect on ice sheet flow, leading to Antarctic ice mass loss of Antarctica and contributing to global sea level rise (IMBIE 2018). Difficulties in accessing the polar regions has created a general scarcity of in situ observations, impeding our progress in understanding ocean heat and salt variability from the Southern Ocean to Antarctic shelf seas, and limiting our ability to evaluate models and theories of its interaction with the atmosphere, sea ice and the Antarctic ice sheet (Akhoudas et al. 2023). With the increasing number of hydrographic profiles now broadcasted on an almost daily basis from the Southern Ocean via satellite, and recognising the somewhat specialized nature of the observations made in polar regions which tends to fall outside of the center of attention of other compilations and climatologies (e.g., WOD, EN4), the time is ripe to create a broad compilation of profile observations and an associated ocean climatology (see also Yamazaki et al, 2025) .

In this paper, we will present two sets of data products that are generated under the OCEAN ICE (O:I) project. The first dataset is the standardised O:I hydrography profiles compilation that assembles temperature and salinity profiles taken from historical CTD stations, Argo floats and instrumented-seal tags. These profiles undergo a standardisation including quality and duplication checks and are formatted in a coherent data structure that is easy to use and update. The second dataset is the O:I Southern Ocean hydrography climatology (Fig. 1b) generated using the O:I profile compilation and a newly-developed objective analysis method that provides a better representation of the Antarctic shelf seas which to date has been more sparsely sampled and represented in climatologies. The paper is organized as follows. First, we introduce the data source and standardisation procedure that is applied to the profile compilation (section 2). In section 3, we discuss some perspective on the analysis of temporal variability that this profile compilation can potentially provide. Generation and evaluation of the O:I climatology is described in section 4, followed by a short summary in section 5, where we discuss a set of future research avenues offered by the new datasets.

https://doi.org/10.5194/essd-2025-727
Preprint. Discussion started: 16 January 2026

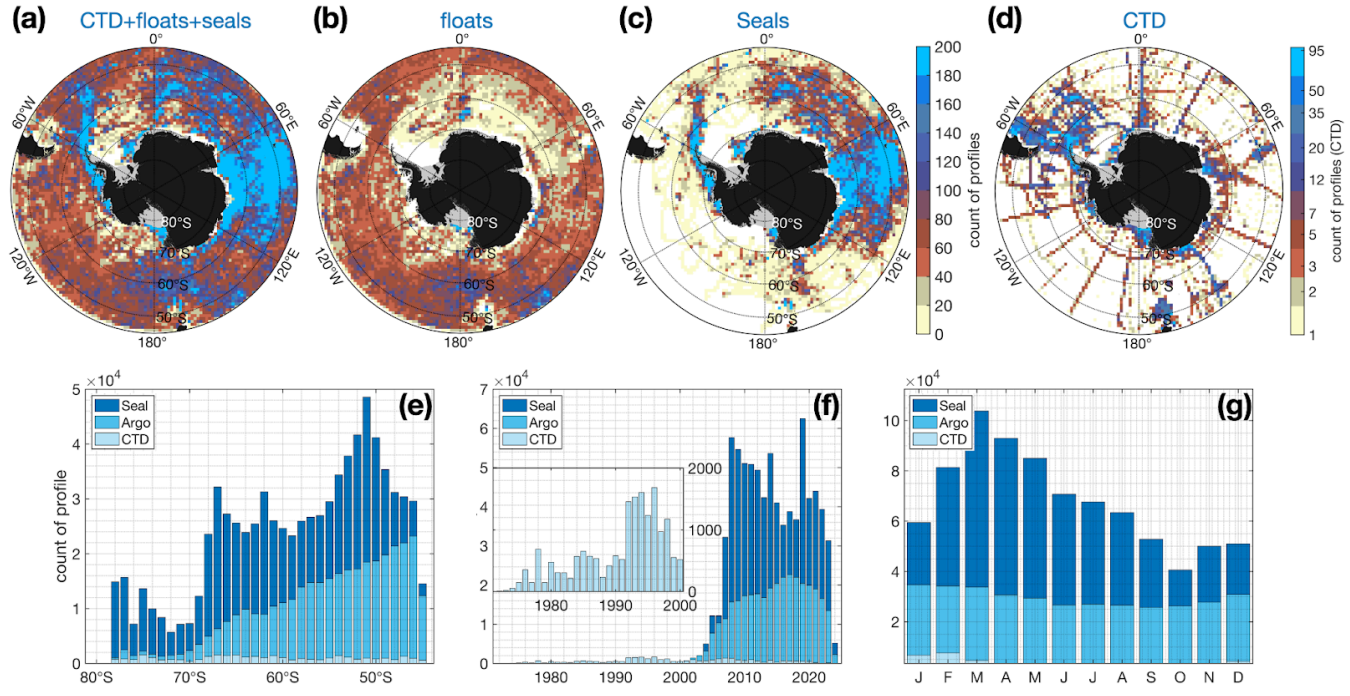

Figure 2. (a)-(d) Number of non-duplicate profiles within 100×100 km boxes South of 45°S aggregating a combination of different data sources indicated in subplot titles, note that the CTD profile counts are shown in a logarithmic scale. Stacked bar plots showing (e) the zonally integrated profile count over different latitude bands, (f) yearly profile count with a focus on the 1970-2000 time period in inset, and (g). monthly profile count.

2 Data and Method

2.1 Data sources

The temperature and salinity profiles compilation that was used for constructing the new Southern Ocean climatology consists of three data types. Ship-based CTD, Argo float profilers and instrumented seal data that are obtained over south of 45°S. Ship-based CTD data from the World Ocean Database (WOD) were accessed on 19 December 2023, therefore new CTD casts from the 2023-2024 season are currently excluded from this compilation. Additional CTD casts from other databases such as the CLIVAR and Carbon Hydrographic Data Office (CCHDO), the British Oceanographic Data Centre (BODC), SODB (Orsi and Whitworth, 2005), the Korean Polar Data Center (KPDC), Pangaea Data publisher and the Norwegian Polar Data Center (NPDC). Argo data were accessed through US GODAE (https://nrlgodae1.nrlmry.navy.mil/cgi-bin/argo_select.pl) on 23 August 2024, and include both the delay-mode profiles and real-time profiles to maximise the sampling on the continental shelf. Quality-controlled instrumented seal data are obtained from the MEOP database (Roquet et al. 2024), and were last accessed in November 2024.

https://doi.org/10.5194/essd-2025-727
Preprint. Discussion started: 16 January 2026

2.2 Data curation and standardisation

Only profiles south of 45°S are retained in our compilation to focus on the Southern Ocean and Antarctic continental shelves. The profiles are first selected based on their position and date control flag to remove any profiles that have been logged as bad data. Argo floats and instrumented seal data share the same quality control (QC) flag scale (https://www.ukargo.net/data/quality_control/, last access: 23 August 2024), while the WOD ship-based CTD profiles apply a different QC flag scale (Garcia et al. 2018). For ship-based CTD casts obtained from other databases, we follow each of the individual QC flag scales and we only select 'good data' or equivalent. For the Argo float and instrumented seal data, we select profiles flagged as '1' (good data) or '8' (interpolated value) to include under-ice profiles. Location correction on under-ice profiles of Argo floats were investigated previously by assuming coast-following float trajectories near the Antarctic continent (Yamazaki et al. 2020) over the interpolated float positions. This is an interesting avenue of research. Given the limited amount of concerned trajectories to date and a lack of quantification of the positional error, we opted to use interpolated positions for now, but recognize a proper treatment to correct the Argo trajectories both near the coast and in the open ocean is needed. Each profile is then screened using the separate temperature and salinity quality control flags throughout the water column and we retain only flagged-good data points within each profile.

Following profiles selection, conservative temperature and absolute salinity are computed using the TEOS-10 GSW toolbox (McDougall and Barker 2011) and each profile is bin-averaged over a standard pressure from 0 to 6000 dbar using a 10-dbar interval. Ship-based CTD profiles arising from different databases are further cross-referenced to remove potential duplicates using a temporal window of 12 hours and a spatial window of 1 km – if duplicated profiles are found, the profile with greater depth and finer vertical resolution is retained (following Schmidtko et al. 2014). Otherwise only one of the profiles is retained. Pressure levels without observations are filled with NaNs to obtain a uniform dimension in the vertical and form a $M \times N$ matrix (M stands for the total number of profiles and N stands for the number of standard pressure levels, here 601). Profiles of conservative temperature and absolute salinity are stored in two separate NetCDF files to accommodate a more user-friendly file size. Extra data information crucial for traceability is also provided in the NetCDF file, including the data sources and instrument types (Table 1). In total, 818,969 temperature/salinity profiles are compiled, among which 33,946 are ship-based CTD profiles, 320,256 are Argo profiles and 465,416 are instrumented seal profiles. Figure 2 illustrates the spatial and temporal complementarity of the various data sources, mentioned above. This compilation is now published with SEANOE (https://doi.org/10.17882/99787, last access: 28 September 2025) and freely available and subject to regular (~annual) update.

Variable names	Attributions and units
lat	Latitude [-90, 90] (°)
lon	Longitude [-180,180] (°)

https://doi.org/10.5194/essd-2025-727
Preprint. Discussion started: 16 January 2026

Open Access Earth System Science Data Discussions

dyr	Days since 1950-01-01 00:00:00
source_flag	Data source indices, 1=WOD, 2=SODB, 3=KPDC, 4=CCHDO, 5=BODC, 6=Pangaea, 7=Argo, 8=MEOP.
instrument_type_flag	Instrument type indices, 1=CTD, 2=OSD, 3=XBT, 4=MBT, 5=Argo profiler, 6=instrumented-seal profiler
pres	Standardised pressure level (dbar)
ct/sa	Conservative Temperature (°C)/Absolute Salinity (g/kg)
bathy	Local water depth from RTopo (2.0.4)/CTD cast readings (m)
doi	External source links. The unique cast IDs are given for WOD sourced CTD casts, cruise codes and PI names are given for CTD from KPDC. Otherwise, the downloadable data links are provided.
access_date	The date of access to data centres (in days since 1950-01-01 00:00:00)

Table 1. Variables in compiled profiles NetCDF file.

3 Exploration of sampled temporal variability

The spatial and temporal sampling inhomogeneity of these hydrographic profiles makes it challenging to utilise the profiles collected for temporal variability analysis, as oceanic conditions on the continental shelves and in the deep Southern Ocean are highly region-dependent, separated by dynamic barriers, and therefore may not be prone to respond in phase to climatic forcing. As such, attempts to explore the long-term oceanic trends on multidecadal timescales over broad regions provide some informative results (Schmidtko et al. 2014) but often have to convolve the spatial and temporal variability that we understand to be a feature of the complex atmosphere-ice-ocean interactions in Antarctic shelf seas (Jenkins et al. 2018). Given the presence of large spatial gradients between shelf seas and the Southern Ocean, for example, one has to be careful not to attribute mean steady spatial gradients to temporal variations, and inversely. In the following, we develop a simple metric aiming to inform on the distance around a centre location one has to assume dynamic consistency to discuss temporal trends and variability in statistically meaningful ways.

https://doi.org/10.5194/essd-2025-727
Preprint. Discussion started: 16 January 2026

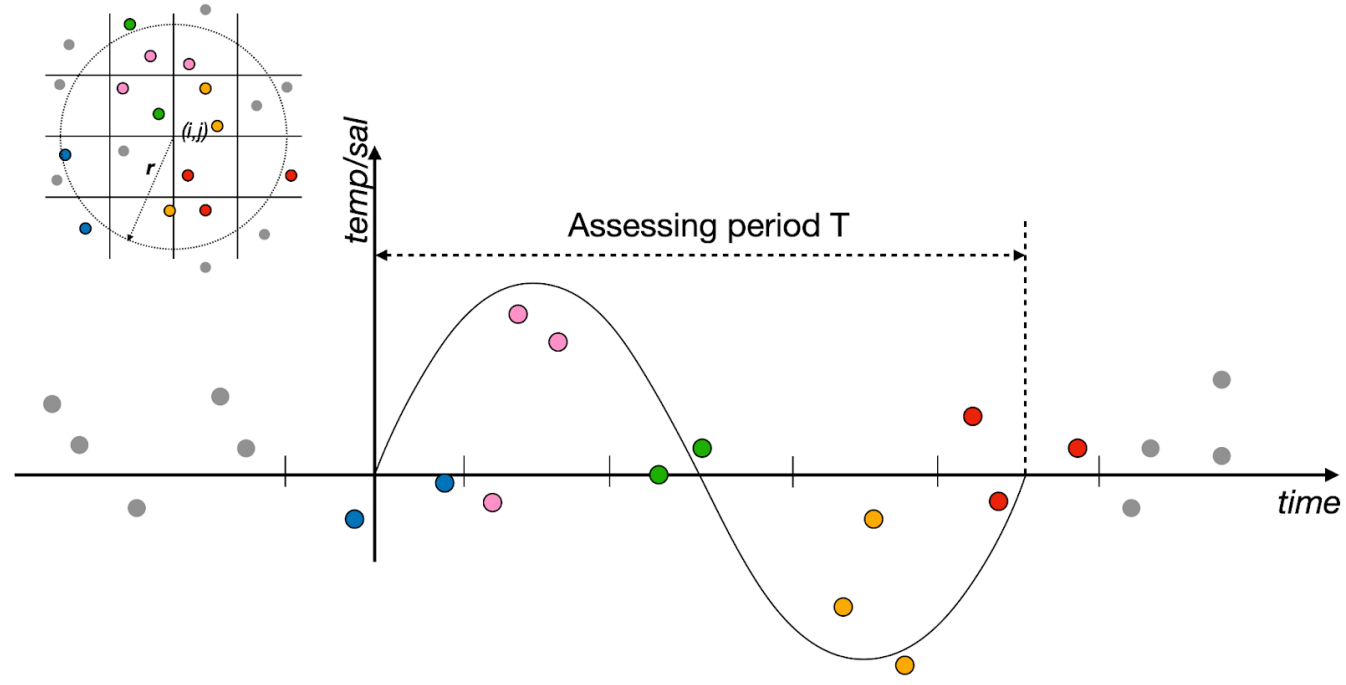

Figure 3. Schematics depiction of an idealized spatial and temporal distribution of profiles. The spatial distribution of the hydrographic profiles (colored dots) from a central location with coordinate (i,j) is shown in the top left inset. The temporal distribution of the same number of profiles over the assessing time period is presented. The assessing period T is evenly decomposed into 5 segments to evaluate the ability of the temporal sampling to estimate a simplified sinusoidal signal within period T.

Assuming variability in the form of simple sinusoids of period T, the minimum sampling required to eventually capture or fit such variability requires one sample within each quintile evenly distributed throughout said period T (Fig. 3). The assessing period can then be moved over time to cover the entirety of the observational window of interest (in our case, from 1972 onwards). In an ideal world, all samples would be obtained within a self-contained, minimal dynamic entity, typically one single ocean location in areas where ocean dynamics is strongly tied to seabed/ice base geometry. In practice, however, repeat observations are seldom obtained at the same location, so one has to expand its search radius r (Fig. 3, inset) to increase the number of samples considered for the analysis. For a period T, starting from an initial search radius r=5 km, a sliding window T looks for one realization where each quintile is sampled. If such a realization is found, the search is completed. If not, the search radius is increased by increments of 5 km and the process continues until a realization is found or the search radius reaches 2250 km, and in which case it is safe to assume that the temporal sampling does not correspond to a single coherent dynamic entity.

In practice, we divide the whole domain (south of 45°S) into evenly spaced boxes with 10 km box size. Then at each grid point (*i,j*), we performed the search for an individual window T using the following steps:

https://doi.org/10.5194/essd-2025-727
Preprint. Discussion started: 16 January 2026

Step 1. Determine assessing period T: e.g., 30-yr period over any point between 1972 and 2024. Start the following steps by placing the assessing period window at the beginning of the observing period, i.e. year 1972.

Step 2. Searching for data within a 5 km radius circle centred at (*i*,*j*) containing at least one data point in each of the five segments within the given assessing period.

Step 3. If **Step 2** is not fulfilled, expand the radius by 5 km incrementally until **Step 2** is fulfilled. If **Step 2** is not fulfilled by the searching radius exceeding the entire domain, we then take the searching radius as ~5500 km, which is the radius of the entire domain.

Step 4. Record the searching radius returned from **Step 2** and **Step 3** and then move the assessing period window (e.g., the 30-yr period) 45 days forward and repeat **Step 2** and **3**. This step therefore records all the searching radius determined for different assessing period windows sliding along the entire observing period from 1972 to 2024.

Step 5. Record the minimum radius (searching range) from **Step 4** for mapping.

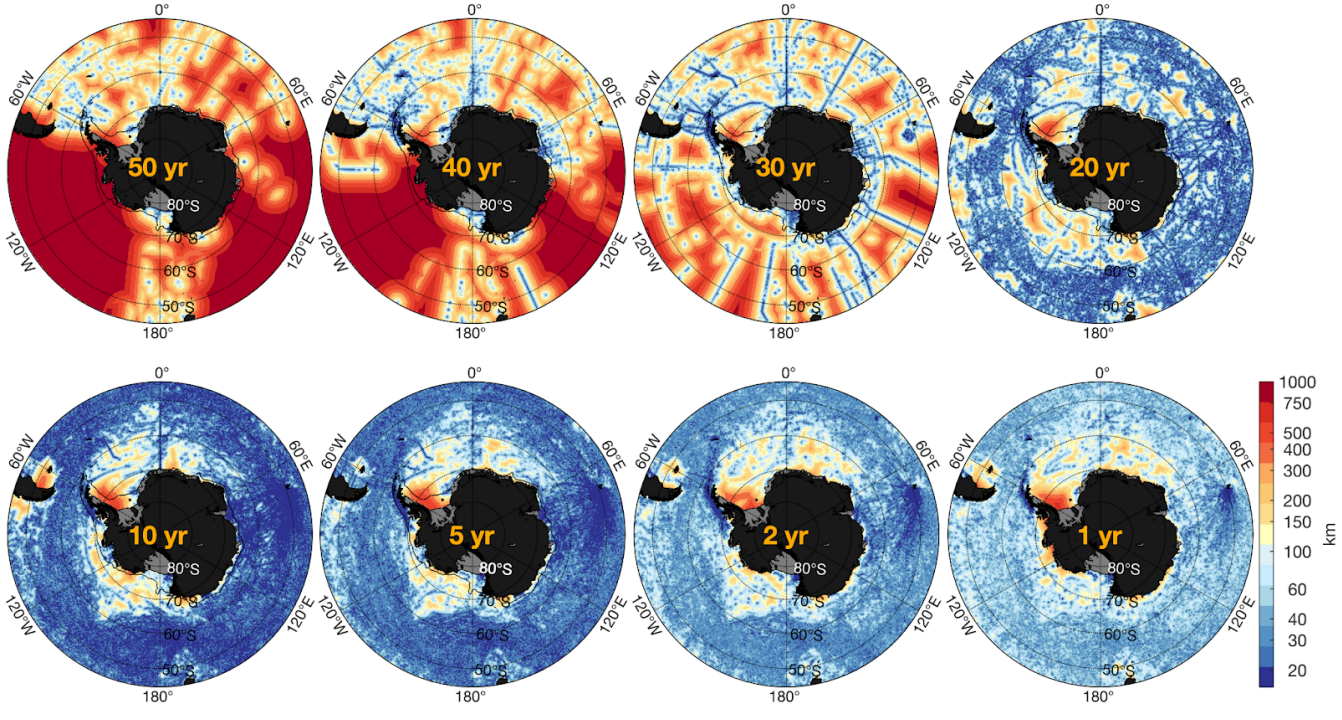

Figure 4. The searching range map for eight various assessing periods of choice from 1 year to 50 years. This covers the timescales ranging from seasonal to multidecadal timescales.

The algorithm provides a search range (in km) at each grid point that represents the minimum searching radius needed at this point to include sufficient temporal samples to observe a sinusoidal variability. Such search ranges are obtained for different assessing periods (T), varying from 1-year to 50-year, to evaluate the ability of the present compilation to quantify variability over seasonal to multidecadal timescales (Fig. 4). Over multidecadal timescales (30-50 year), small searching ranges are largely constrained by the location of early historical samples from ship-based CTD casts indicated by the blue stripes

https://doi.org/10.5194/essd-2025-727
Preprint. Discussion started: 16 January 2026

following WOCE track lines. We note that there is a decent temporal coverage with limited (<100 km) search radius over many continental shelves for 2 to 30-year time periods, in the southwestern Weddell Sea continental shelf, Dronning Maud Land, Cosmonaut Sea, Vincennes Bay, Adelie Land, the Ross Sea, the Amundsen Sea, the Bellinghausen Sea and the West Antarctic Peninsula. At seasonal timescales, the shelf seas are typically poorly sampled primarily because of the dominance of CTD casts that were collected during summer months or the fact that instrumented-seal sensors only cover roughly eight months across the year between the time separating the sensor installation and the following seal moulting season. It is therefore likely that some of the more poorly sampled months of September-November will lack sufficient coverage to create a dynamically consistent view of a monthly climatology. The Ross Sea continental shelf, on the other hand, displays good data coverage throughout all timescales. Here, the decent seasonal coverage is due to Argo float profilers that were deployed over the continental shelf and parked on the seabed between profiles, limiting drift and acting as virtual mooring sampling the area throughout the year.

4 OCEAN ICE (O:I) climatology

Keeping the caveats related to spatio-temporal sampling noted above in mind, we nevertheless provide new climatologies of the mean state of temperature and salinity south of 45°S. Focusing on the Southern Ocean and Antarctic shelf seas, the large-scale distribution of the temperature and salinity in the Southern Ocean has been described by previous versions of Southern Ocean climatologies such as the Southern Ocean Atlas based purely on ship-based measurements such as CTD and bottle samples (Orsi and Whitworth 2005) or more recently by assembling data from both ships, Argo floats (Schmidtko et al. 2014) and instrumented seals (Yamazaki et al 2025). Except for the latter, all of these climatology products adopt optimal estimation of the temperature and salinity field to map the water properties from scattered data points. In our climatology, we use the notion of ‘ellipse of influence’ around designated climatological grid points to obtain a mean local state of the ocean, which is inspired by the method used in the Southern Ocean Atlas, but with some refinements discussed in the following.

4.1 Interpolation scheme

In the Southern Ocean Atlas, it was assumed that circulation in the interior of the Southern Ocean was mainly zonal, such that tracers would remain fairly uniform and could be averaged over ellipses with their main axis aligned in the zonal direction. Each ellipse was further characterized with a fixed 2:1 anisotropy in zonal:meridional correlation length scales, and the length scales were designed to accommodate local bathymetry - 666:333 km in deep ocean with the bottom depth greater than 4000 m, 444:222 km in places where water depth varying between 1000 and 4000 m to account for ocean ridges and finally 222:111 km in shelf seas shallower than 1000 m, further assuming that horizontal length scales were dynamically tied to water column height. With the advent of satellite observations and data assimilation models, improved understanding of ACC meanders, the presence of quasi-steady gyres arrested by topographies, we are now able to refine our assumptions

https://doi.org/10.5194/essd-2025-727
Preprint. Discussion started: 16 January 2026

about the direction of the main ocean circulation to maximize the representation of gyre-scale features and the effect of local bathymetry. We can also add the complementary float and seal profiles.

For the O:I climatology, instead of applying zonally oriented ellipse clusters, the orientation of each ellipse is determined using the sea surface height (SSH) contour, here used as a proxy for the barotropic component of the ocean circulation (Fig. 5a). The SSH is provided by the 139th iteration of Southern Ocean State Estimate (SOSE, Mazloff et al. 2010), which assimilates observations not only temperature/salinity profiles but also the mooring time series and surface measurements such as the observed sea surface height, temperature, salinity and sea ice concentration. The SSH field therefore covers the sea-ice area and provides a dynamically conserved estimation of the large-scale barotropic ocean circulation. With improved spatial sampling, we also adjust the size of the ellipse, reducing the correlation length scales compared to those used in the Southern Ocean Atlas. In our algorithm, the largest correlation length scale is 290:145 km in the deep ocean with water column thickness in excess of 4000 m, 267:138 km between 4000 m and 3000 m, 178:89 km between 3000m and 2000m, 89:44.5km between 2000 and 1000 m. Small ellipses with the aspect ratio of 44.5:22.2 km are applied everywhere where the water column thickness is lower than 1000 m which we regard as continental shelf regions (Fig. 5b). RTopo 2.0.4 (Schaffer et al. 2016) is used to provide the bathymetry information needed for determining correlation length scales for each ellipse. The orientation of the ellipse on the continental shelf follows the local topography gradient due to the deterioration of the SOSE SSH robustness associated with the lack of reliable assimilated data, model resolution, and representation of ice shelf ocean interactions (Mazloff 2010).

The climatology is constructed on a 0.2°×0.1° (longitude×latitude) grid. The choice of the horizontal resolution is to accommodate the shelf ellipse size so that the neighbouring ellipse has a certain degree of overlapping to avoid missing sampling data points. At each grid point, our initial approach for obtaining averaged representative values consists in using a weighting matrix based on the distance from target location distorted by the elliptical fields described above. The weighting is formulated as

$$w_{SODB} = e^{-[(\frac{\Delta d_M}{M})^2 + (\frac{\Delta d_m}{m})^2]},$$

where Δd_M is the horizontal distance of a data point to the major axis of the ellipse, M is the length of the ellipse major axis. Δd_m is the horizontal distance of a data point to the minor axis of the ellipse, and m is the length of the ellipse minor axis..

https://doi.org/10.5194/essd-2025-727
Preprint. Discussion started: 16 January 2026

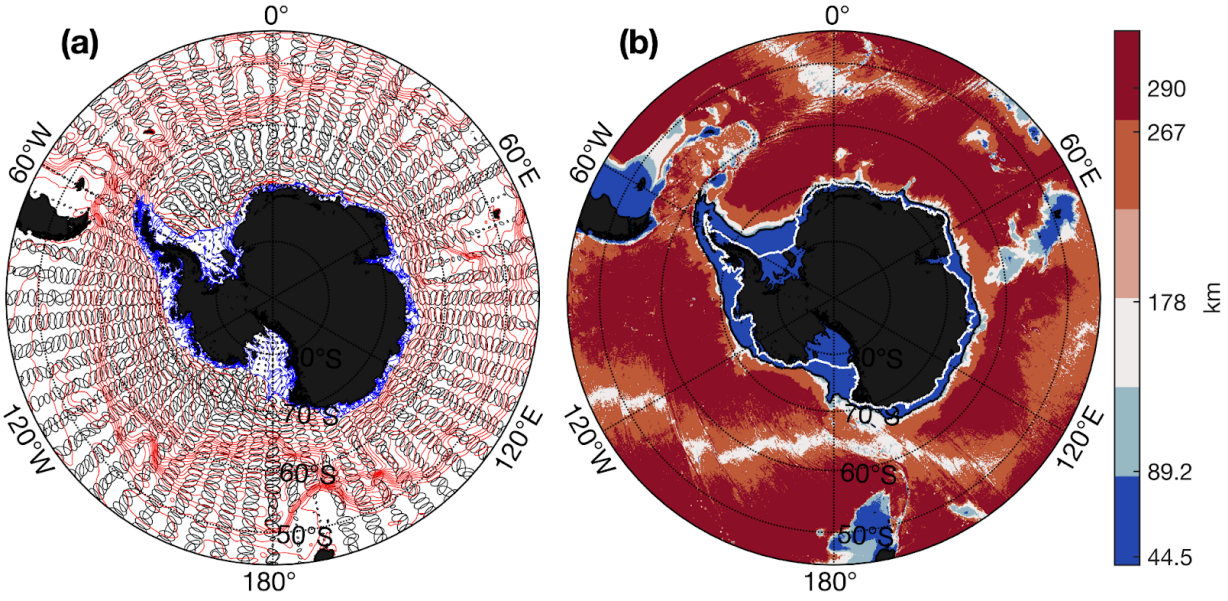

Figure 5. (a) Black ellipse polygons are the coarse-grained ellipses distribution of the interpolation scheme. Red contours are the time-mean SOSE SSH contours north of the 1000m isobath and the blue contours show the continental shelf topography. The ellipses are oriented along-stream of SOSE SSH contours off the shelf and seabed topography on the shelf to account for more detailed dynamic coherence and distinguish the different dynamic regimes on and off the continental shelf. (b) The spatial distribution of the correlation length scales depicted by the major axis length of ellipses.

This method is adequate for sufficiently sampled regions, and those where bathymetric constraints on flow are taken into account by ellipse orientations, i.e. intermediate to surface Southern Ocean. It is however more problematic in sparsely sampled regions and those where bathymetry plays a significant role in water mass properties horizontal anisotropy (e.g. the continental shelf). To alleviate this issue, a fast-marching (FM) algorithm is performed to search for and select data beyond the spatial bound defined by ellipses, thereby filling gaps in sparsely to unsampled regions where a simple average metric within ellipses loses meaning. FM algorithms have been previously adopted, for example, in constructing Monthly Isopycnal and Mixed-layer Ocean Climatology (MIMOC, Schmidtko et al. 2013), and bears the advantage of a reasonable consideration of topography-steered currents dominating the Antarctic continental shelves, by measuring data point distance along the isobath derived from a given bathymetry and applying extra penalty on data points that are sitting across isobaths. The FM weighting matrix associated with the along-path distance is formulated as

$$w_{FM} = e^{-[(\frac{\Delta d}{L_d})^2]},$$

where Δd is the along-path distance given by the FM algorithm and L_d is the decorrelation length scale of the Gaussian weighting function, here set to 400 km to be equivalent to the open ocean ellipse length scale. Note that we further limit our FM average to the top 1000 weighted data points, for computational efficiency.

https://doi.org/10.5194/essd-2025-727
Preprint. Discussion started: 16 January 2026

Our final product incorporates the FM algorithm with our SODB ellipse-based interpolation scheme to retain the capability of resolving spatial gradients within sufficiently densely sampled ellipses and interpolating in more poorly sampled regions. The construction of the climatology field is therefore performed based on the FM selected data points with a spatially-varying weighting strategy combining both the FM-determined along-path distance of data points from the centre of each grid and the horizontal distance between the data points to the ellipses. The relative importance of two sources of weighting is controlled by the number of data points counted within the ellipse at each grid point, favouring the SODB ellipse based method in densely sampled regions. The complete spatial weighting matrix combining the FM and ellipse styles with the consideration of data density is then given as

$$w_D = w_{FM}^{-N^p_{ellipse}} \cdot w_{SODB}^{(1-N^p_{ellipse})},$$

where $N^p_{ellipse}$ is the number of profiles counted within each ellipse in the OCEAN ICE hydrography profiles at each depth. The FM weighting and the ellipse weighting are illustrated as an example in Fig. 6a/b/d.

An optional temporal weighting is designed to provide extra seasonal/monthly constraints on climatological fields. Fig. 6e shows the temporal weighting centred around the month January which is regarded as austral mid-summer on average. The temporal weighting is given as

$$w_\tau = e^{-[(\frac{\Delta\tau}{L_\tau})^2]},$$

where $\Delta\tau$ is the time difference of the data point from the given month (mid-January, central month = 0.5), and L_τ, set to be 2.5 months, is the decorrelation timescale. For our summer climatology construction, the weighting matrix is then given as $w_{summer} = w_D \cdot w_\tau$.

The results herein are mainly based on the full climatology without temporal weighting, and we only briefly show the difference between the full and summer climatology later. A third climatology is created and available using only the data after 2000 with a focus on the 'contemporary' period when the data acquisition is dominated by the advent of Argo floats and instrumented-seal profiles, and which may be useful for some numerical model comparison exercises. A zoomed in view of the constructed full climatological conservative temperature maximum field in Amundsen Sea Embayment (Fig. 6f) shows strong lateral gradients across the continental shelf over a few kilometres. The stripe of circles and ellipses in Fig. 6f showcases the ellipse size variation from the continental shelf to the open ocean. Within reason, the size of circles on the continental shelf is fine enough to resolve lateral gradients, lending credence to our choice of correlation length scales over the continental shelves. To quantify the error of the climatology product, a modified standard error to show the spatial distribution of data in contributing to the data uncertainty ($MSE_{spatial}$) is computed by scaling the weighted standard deviation, σ_w, with the number of valid data points counted in the ellipses, $N_{ellipse}$,

https://doi.org/10.5194/essd-2025-727
Preprint. Discussion started: 16 January 2026

$$MSE_{spatial} = \frac{\sigma_w}{\sqrt{N_{ellipse}}}.$$

Note that the $N^p_{ellipse}$ and $N_{ellipse}$ are two different metrics. The former represents the number of casts in each ellipse which is a depth-independent metric while the latter is the count of valid data points in each ellipse at each depth. $N^p_{ellipse}$ is used to constrain the relative contribution to the total distance weighting from FM and ellipse algorithms at each grid point, such that the weighting metric is kept uniform in depth instead of using the depth-varying $N_{ellipse}$ that tends to weigh more on FM strategy over the ellipse strategy and leads to overly smoothed temperature and salinity field than desired. The MSE of the conservative temperature at 100 dbar in the Amundsen Sea Embayment is shown in Fig. 6g, where the dark red marks point to the large MSE region where the produced climatology value suffers from large uncertainty due to the lack of data points. For the summer climatology, the modified standard error (MSE_{summer}) is computed using the number of the data points collected from November to March, corresponding to the central month and decorrelation time scale used for summer climatology, N_{summer},

$$MSE_{summer} = \frac{\sigma_w}{\sqrt{N_{summer}}}.$$

https://doi.org/10.5194/essd-2025-727
Preprint. Discussion started: 16 January 2026

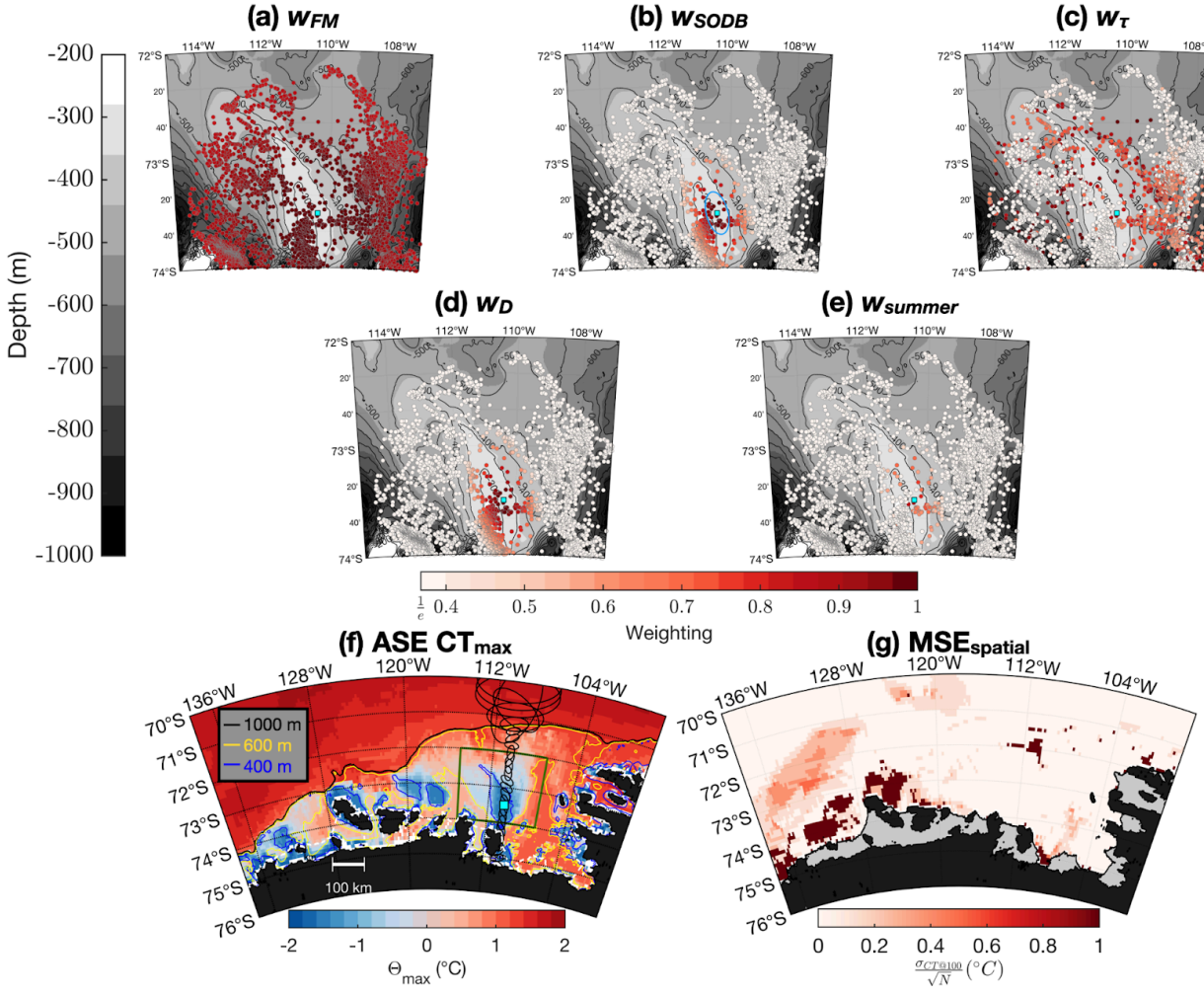

Figure 6. (a) The weights (ranging from 0 to 1) defined by along-path distance, w_{FM}, computed by FM algorithm over the climatology grid at 110.4°W, 73.5°S. Colour shading of the data points denotes the value of weights, the redder the colour is, the more weight is assigned. Cyan square denotes the centre location of the inspected climatology grid cell. The gray shades in the background and black contours show the bathymetry from RTopo. (b) to (e) are the same as (a) except that the data points are coloured according to the ellipse size weighting w_{SODB}, month weighting w_{τ} (with the given month being January), combined distance weighting w_D, and combined summer weighting w_{summer}, respectively. Blue polygon in (b) denotes the ellipse used to compute the w_{SODB} at the highlighted grid point. (a)-(e) only plotted the location of first 100 data points with highest combined distance weighting, w_D. (f) shows the maximum conservative temperature in the Amundsen Sea Embayment from the O:I climatology. The continental shelf break is highlighted by the 1000 m isobath (thick black contour) and bathymetric contours are overlaid in yellow for 600 m and blue for 400 m. Ellipses exemplify the choice of ellipse size along a longitudinal transect constrained by the local water depths on the continental shelf and SSH contour off the

https://doi.org/10.5194/essd-2025-727
Preprint. Discussion started: 16 January 2026

shelf break. (g) shows the modified spatial standard error ($MSE_{spatial}$) for conservative temperature at 100 dbar in the Amundsen Sea Embayment, with dark red regions denoting high interpolation uncertainty, hence low confidence in the climatology.

4.2 Cabbeling correction

The cabbeling effect due to the nonlinearity of seawater's state equation leads to artificially created dense water masses when taking average over temperature and salinity fields. In the case of an isopycnal climatology product (Schmidtko et al. 2013), the mixing process can be represented by taking average over the temperature and salinity field along isopycnal coordinates. The cabbeling correction on temperature and salinity can be then derived following

$$\Delta\Theta = \frac{\sigma\left(S_{Amap},\Theta_{map}\right)-\sigma_i}{2\alpha\rho_0} \text{ and } \Delta S_A = -\frac{\sigma\left(S_{Amap},\Theta_{map}\right)-\sigma_i}{2\beta\rho_0}.$$

Here S_{Amap} and Θ_{map} are mapped salinity and temperature along the initial isopycnal coordinate σ_i, α and β are local thermal and haline expansion coefficients and ρ_0 is the reference density. In our case, temperature and salinity are averaged over pressure coordinates, therefore there is no reference isopycnal to quantify the density changes raised by the cabbeling effect. Instead, we crudely use the averaged in-situ density as our reference density. In this case, the density correction to be applied is simply the difference between the averaged in-situ density, $\overline{\rho\left(S_A,\Theta,p\right)}$, and the density computed using averaged temperature and salinity, $\rho\left(\overline{S_A},\overline{CT},p\right)$,

$$\Delta\rho = \rho\left(\overline{S_A},\overline{\Theta},p\right) - \overline{\rho\left(S_A,\Theta,p\right)},$$

where the $\overline{\Theta}$ and $\overline{S_A}$ are the weighted mean value of the temperature and salinity estimated by the objective mapping as above. The adjustments of temperature and salinity required to effectuate this density change, under first-order approximation, are

$$\Delta\rho = \frac{\partial\rho}{\partial\Theta}\Delta\Theta + \frac{\partial\rho}{\partial S_A}\Delta S_A.$$

The above can be treated as the single linear constraint for estimating the temperature and salinity adjustment. To minimize the adjustment on temperature and salinity field while complying with the density correction constraint above. We treat the problem as a least-square minimization problem where the cost function of the minimization is represented as the total adjustment on temperature and salinity estimated as $J = \Delta\Theta^2\left(\frac{\alpha}{\beta}\right)^2 + \Delta S_A{}^2$. Note that we weighted the conservative temperature adjustment with the ratio $\frac{\alpha}{\beta}$ to arrive at the same unit as the absolute salinity. Since this is a linear minimization problem with one linear constraint and a quadratic cost function, the temperature and salinity adjustments can be analytically estimated as,

$$\Delta\Theta = -\frac{\Delta\rho}{2\alpha\rho} \text{ and } \Delta S_A = -\frac{\Delta\rho}{2\beta\rho}.$$

https://doi.org/10.5194/essd-2025-727
Preprint. Discussion started: 16 January 2026

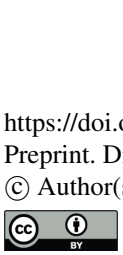

Open Access Earth System Science Data Discussions

Fig. 7 illustrates the cabbeling corrections applied on conservative temperature (Fig. 7a) and absolute salinity (Fig. 7b) fields to rectify the cabbeling effect on the density field quantified as the density difference between the density computed from averaged temperature and salinity and the averaged in-situ density (Fig. 7c) at 1000 dbar. Some of the strongest nonlinear mixing biases are found in the core of the Antarctic Circumpolar Current (ACC), bounded by the Subantarctic front and southern ACC front, with regional hotspots of larger bias coinciding with the reported enhanced upwelling locations forced by local topographic feature (Tamsitt et al. 2017). The effect of T-S relation adjustment is shown in Fig. 7d over the locations denoted in Fig. 7a. The T-S adjustment resembles those found in Schmidtko et al. (2013) where the cabbeling effect is well-defined in isopycnal-averaged temperature and salinity fields. The cabbeling correction is mostly discernible over shallower depths where the temperature and salinity experience larger variance along the isopycnals.

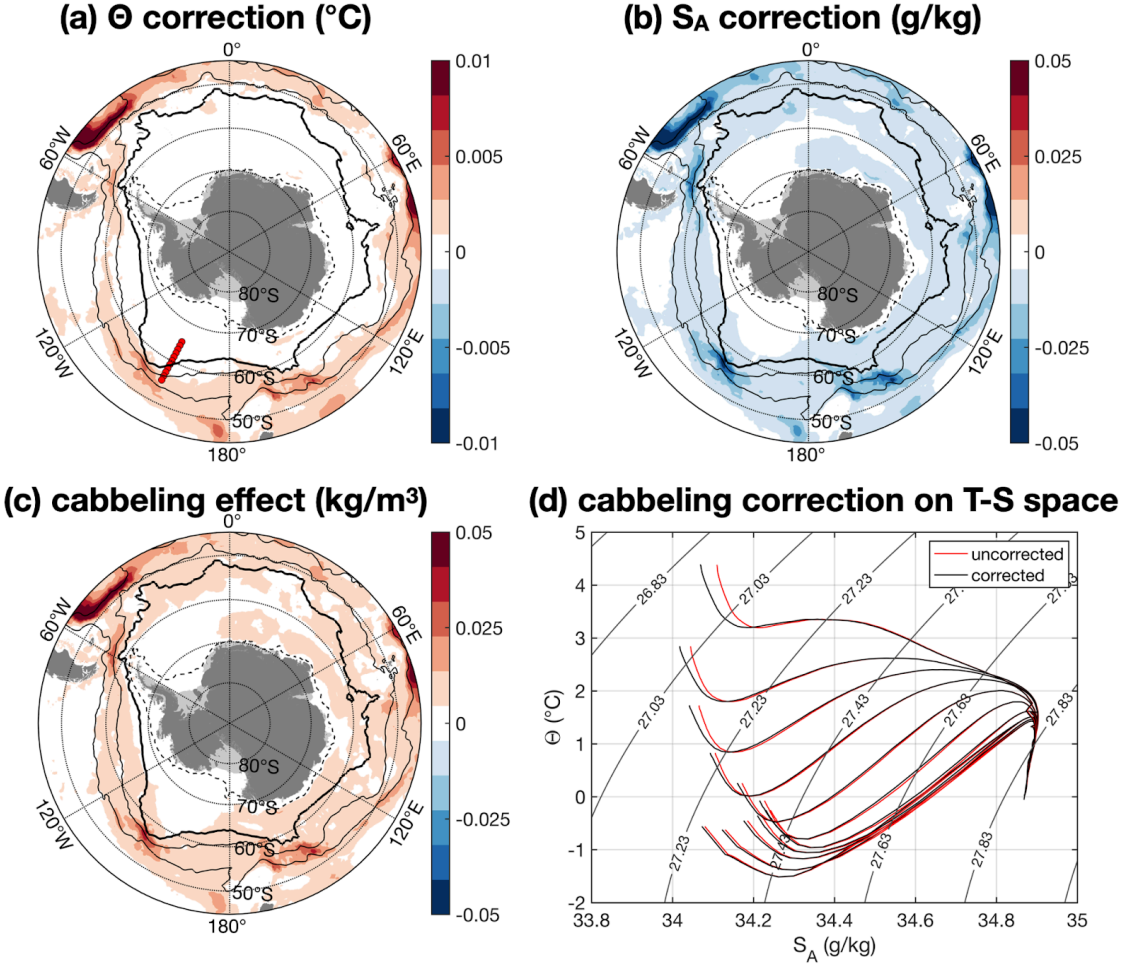

Figure 7. The cabbeling correction of (a) conservative temperature, (b) absolute salinity and (c) the cabbeling effect on the in-situ density at 1000 dbar. (d) the adjustment of T-S by cabbeling correction over the 10 selected locations denoted in (a) by red circles, background contours are potential density. Thick black contour in panels (a) to (c) denotes the southern Antarctic Circumpolar Current front, two thin contours further north denote the (from south to north) polar front and sub-Antarctic front (Kim and Orsi 2014).

https://doi.org/10.5194/essd-2025-727
Preprint. Discussion started: 16 January 2026

4.2 Density stabilisation

Climatologies created in isobaric spaces are prone to create interpolation-derived density inversion. Some form of density stabilisation is therefore needed, assuming that density inversion is not a sensible stable state (e.g. Ridgway et al, 2002, Boyer et al. 2005, Locarnini et al. 2013). Various methods have been developed by the community, often solving a nonlinear minimization problem (Jackett and Mcdougall 1995, Chu and Fan 2010, Wang et al. 2012, Barker and McDougall 2017) to minimise temperature and salinity correction while achieving stabilization with the least adjustments possible. In our climatology, before cabbeling correction, we first locate profiles with unstable density structure. The criterion for detecting unstable water column is formulated as the following (Chu and Fan, 2010),

$$E < 0,$$

where E is the measure of the water column stability represented by the vertical density gradient. For discrete sample (T_k, S_k) at depth z_k (k = 1, 2, …), E_k is obtained as the difference between two adjacent levels,

$$E_k = \rho\left(T_{k+1}, S_{k+1}, z_k\right) - \rho\left(T_k, S_k, z_k\right),$$

which is density difference between the local potential density of a water parcel at z_{k+1} that the water parcel would acquire if it was adiabatically brought to a reference depth (z_k), $\rho\left(T_{k+1}, S_{k+1}, z_k\right)$, and the in-situ density at z_k, $\rho\left(T_k, S_k, z_k\right)$. E_k is then defined as the local static stability (Lynn and Reid, 1968). In practice, it is not always possible for the discretely measured temperature and salinity to reach a static stability at zero due to the precision of these measurements. A minimum stability, E_{min}, is therefore user-defined to be a small positive value (Chu and Fan 2010, Wang et al. 2012). We choose 10^{-7} kg/m^3 for E_{min} to locate the profiles with unstable density structure and apply two types of stabilisation corrections (see below). In our climatology, before density stabilisation, over 80% of gridded profiles have at least one pair of unstable T-S measurement (Fig 8a) and on average the water column is unstable near the bottom of the water column. This is potentially a common issue of the isobaric average in the deep ocean where the weighted-mean is performed over a pool of CTD profiles with different local bottom depth hence different measuring depth range (Fig. 8b).

https://doi.org/10.5194/essd-2025-727
Preprint. Discussion started: 16 January 2026

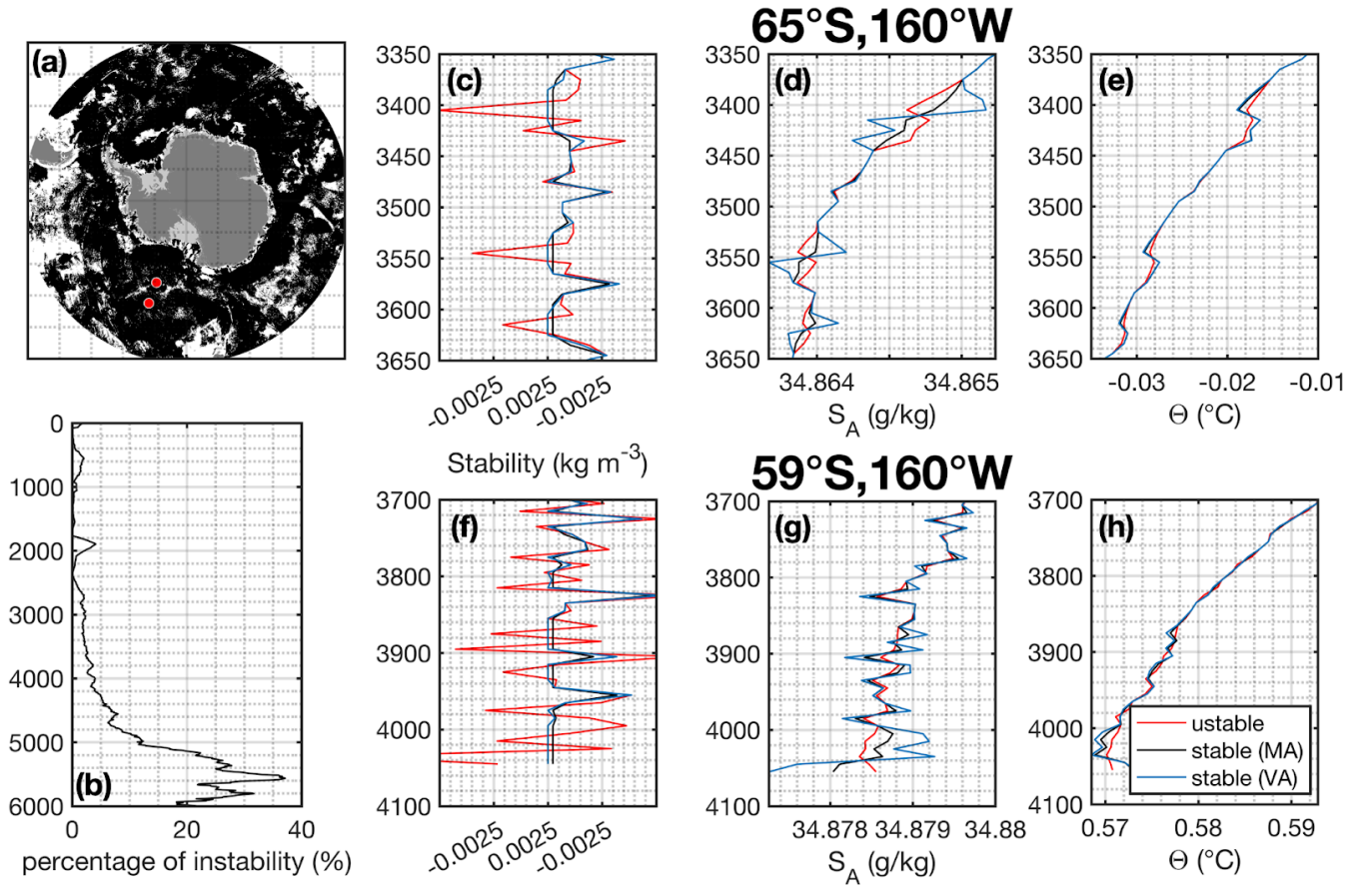

Figure 8. (a) locations of unstable profiles shown as black shade where at least one pair of unstable water parcels is found. (b) Histogram of the number of instabilities as a function of depth in O:I climatology before density stabilisation and the example at 59°S, 160°W (c) - (e) and 65°S, 160°W (f) - (h) showing the (c), (f) stability (d), (g) salinity and (e), (h) temperature before (red) and after the MA (black) and VA (blue) density correction. Locations of example profiles are denoted as red circles in panel (a).

We then compared two most recently developed or refined methods: the Variational Adjustment (VA) scheme by Wang et al. (2012) and an updated Minimal Adjustment (MA) by Barker and McDougall (2017). The MA method uses constrained least squares to minimize the temperature and salinity changes while retaining the T-S coherency by constraining the minimisation problem with a localized linear relation of a representative and smoothed temperature and salinity curve (Barker and McDougall, 2017). The VA method, used in a recent climatology (Yamazaki et al. 2025), is designed to conserve heat and salt content of a water column and preserves T-S coherency determined by the surrounding temperature and salinity field (Wang et al. 2012). While both methods stabilise the water column (Fig 8c and Fig 8f), the VA method tends to overcorrect the temperature and salinity throughout the water column (Fig 8d, 8e, 8g and 8h) and appears to be marginally less effective on rectifying the instability (Fig 8c and Fig 8f) compared to the MA method, as noted in Barker and McDougall (2017). A

https://doi.org/10.5194/essd-2025-727
Preprint. Discussion started: 16 January 2026

detailed description of the MA method and a thorough comparison of the two methods tested in this study along with other conventional density correction methods can be found in Barker and McDougall (2017). To achieve the final form of a statically stable climatology with minimal tampering, we chose the MA scheme and strategically deployed it to profiles where at least one pair of unstable water parcels was detected.

4.2 Evaluation of OCEAN ICE (O:I) climatology

In the following, we provide a brief evaluation of the OCEAN ICE (O:I) climatology using metrics previously built to understand the multidecadal trend of the water masses in the Southern Ocean and on the Antarctic continental shelves, namely the Circumpolar Deep Water (CDW) core temperature, core salinity and core depth and the continental shelf bottom temperature and salinity (Schmidtko et al. 2014). At each horizontal position, the CDW core temperature is defined as the temperature maximum below 100 m to avoid capturing instead surface seasonal warming signatures. CDW core salinity and depth are then defined as the salinity and pressure level where the temperature maximum is observed. The bottom water temperature and salinity on the continental shelf are defined as the average temperature and salinity within 150 m from the seabed.

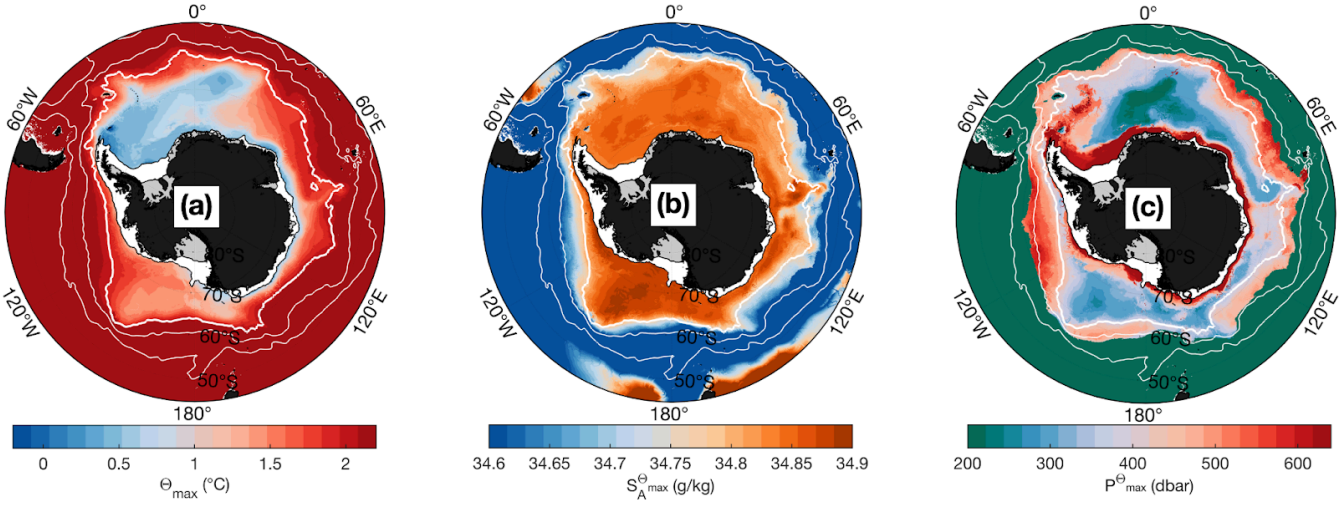

Figure 9. (a) The maximum conservative temperature below 100 m as an indicator of CDW core temperature in the open ocean. Continental shelf is mapped with this metric for completeness. (b) same as (a) but for the absolute salinity at the temperature maximum depth. (c) same as (a) and (b) but for pressure level where the temperature maximum is detected.

Maps of CDW properties in the O:I climatology are shown in Fig. 9. Unsurprisingly, the O:I climatology captures the CDW features (water mass property and position, previously seen in other commonly used climatology products such as the World Ocean Atlas (WOA23, Reagan et al. 2024), with the Weddell and to a lesser extent Ross gyres acting as more or less efficient barriers to the southward ingress of warm CDW towards Antarctic shelf seas. On the continental shelf, bottom water properties are directly compared between the O:I and WOA23 climatologies in Fig. 10 a-f. Overall WOA23 produces

https://doi.org/10.5194/essd-2025-727
Preprint. Discussion started: 16 January 2026

warmer continental shelf bottom water properties, notably in the dense shelves such as in the Weddell Sea and Ross Sea. A vertical section across the Weddell Sea continental shelf break at 37.2°W details differences in dense shelf water representation between the O:I and WOA23 climatologies (Fig. 10g and Fig. 10i). O:I captures a more widespread and thicker cold dense water layer near the sea bed extending across the shelf sea toward the shelf break that is consistent with the understanding and snapshot observations of the dense water overflow arising at this longitude (Nicholls et al. 2009, Darelius et al. 2014). O:I also resolved a more suppressed warm deep water core off the continental shelf in southern Weddell Sea (Fig 10g and Fig 10i), reflecting the contrast between the water mass properties on and off the continental shelf in the dense shelf regime such as in the Weddell Sea where the continental shelf is mostly shielded from modified CDW intrusions (Thompson et al. 2018). As an example of comparison in a warm shelf regime, the difference in bottom water mass properties across a section of the Amundsen Sea continental shelf between WOA23 and O:I climatology are in contrast affected by the different representation of the bathymetry (Fig. 10h and Fig. 10j). But, similarly to its colder regime counterpart, the O:I climatology offers sharper representations of horizontal gradients, with Antarctic slope front clearly tied to the continental shelf break in O:I, in accord with multiple observations (e.g., Walker et al., 2013), whilst it is smeared and much more weakly defined in WOA23. An associated distinguishing feature of the bottom properties difference between WOA23 and O:I climatology is that the WOA23 tends to have a warmer/saltier shelf break (Fig. 10c), which we surmise is associated with a broader scale averaging method used to create the latter and an associated leakage of the warm and saline CDW available offshore to the shelf seas. Indeed, while O:I climatology uses reduced averaging length scales down to 20 km on the continental shelf region, WOA23 smallest influence radii for its interpolation is 200 km (Boyer et al. 2005). Another reason for a warmer/saltier shelf break could be associated with the discrepancies in the bathymetry used in O:I and WOA climatology. For example, the warm water in the latter occupies more fraction of the water column due to the unrealistically deep shelf break in the Amundsen Sea (Fig 10h and Fig 10j) that leads to a warmer/saltier bottom water properties in this region.

https://doi.org/10.5194/essd-2025-727
Preprint. Discussion started: 16 January 2026

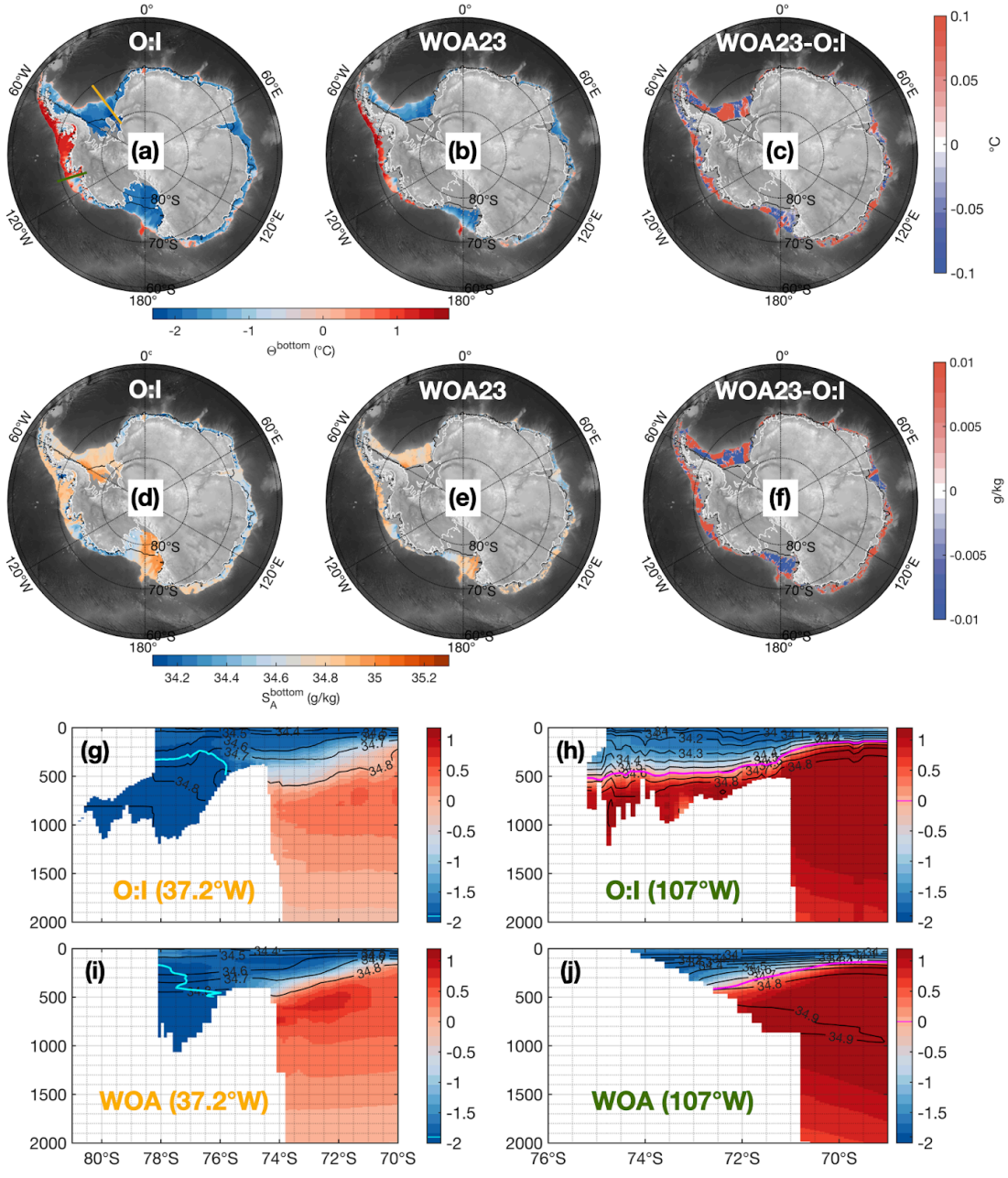

Figure 10. The shelf bottom water temperature/salinity from O:I climatology a/c and WOA23 d/e. Differences of shelf bottom water temperature and salinity between WOA23 and O:I climatology is in c and f. Zoomed-in continental shelf vertical section at Weddell (35°W) derived from (g) O:I climatology and (i) WOA23. (h) and (j) are the same as (g) and (i) but for the Amundsen Sea (107°W). Conservative temperature is shown in colour and absolute salinity is shown in black contours in the vertical section plot. Cyan and magenta thick contours denote the -1.9°C and 0°C isotherm in Weddell and Amundsen Sea, respectively. The locations of two vertical sections shown in (g)-(j) are indicated by green and yellow transect lines in (a).

https://doi.org/10.5194/essd-2025-727
Preprint. Discussion started: 16 January 2026

A comparison of the T-S properties of the continental shelf between the two climatology products is conducted by retrieving regional and circum-Antarctic shelf seas Probability Distribution Function (PDF) in T-S space (Fig. 11). The T-S PDFs are produced from gridded O:I climatology and WOA23 climatology, where the coarser WOA23 climatology is interpolated onto the finer O:I grid and both climatology products are re-masked using the NaN values from both products to ensure the total number of valid temperature and salinity data points are consistent with each other. Regional differences are exemplified in the Weddell Sea (Fig. 11a-c) and in the Amundsen-Bellingshausen Sea (Fig. 11d-f). The raw data used to compute O:I climatology in the Weddell Sea consists of CTD casts near the ice shelf front, and for those obtained in Filchner Trough where one would expect signature of the supercooled Ice Shelf Water (ISW) created by glacial melt as High Salinity Shelf Water (HSSW) interacts with the ice shelf base (Nicholls et al. 2009, Janout et al. 2021, Zhou et al. 2023). ISW is slightly fresher than HSSW but much colder than the local surface freezing point. Such a signature is present in the O:I climatology (Fig. 11a), but absent in WOA23 (Fig. 11c and Fig. 11b) due probably to the over-smoothing by WOA23 objective interpolation. The O:I climatology also possesses a more extensive array of water masses associated with sea ice freezing (data points sitting along the surface freezing line) compared to WOA23 (Fig. 11c) in the Weddell Sea region. A comparison of the thermohaline signature between the O:I full climatology and the O:I Summer climatology is also shown in Fig. 11d, 11h and 11l. Broadly speaking, the main difference between the two products in T-S space shows anomalies along the surface freezing line and anomalous dipoles along lines connecting surface and deeper/denser mCDW end-members in warm shelf regimes (Fig. 11d, 11l). The former difference, a deficit of near-surface freezing counts in summer, is most likely a result of sea ice formation processes not being captured in the summer climatology, as one would expect. This applies to both the HSSW in cold regimes (Fig. 11h) and Winter Water (WW, characterized by temperature minimum near the surface freezing point) in warm regimes (Fig. 11l). We surmise the latter difference reflects seasonal changes in intermediate depth water mass properties, associated with a mix of sea-ice production-driven convection events, and advection (Kimura et al, 2017, Yang et al, 2022). Whilst certainly calling for a more in-depth analysis of seasonal variability, the results we present demonstrate that the temporal weighting can effectively capture and highlight the seasonality in some of the key water masses on the continental shelves over both pan-Antarctic and regional contexts.

https://doi.org/10.5194/essd-2025-727
Preprint. Discussion started: 16 January 2026

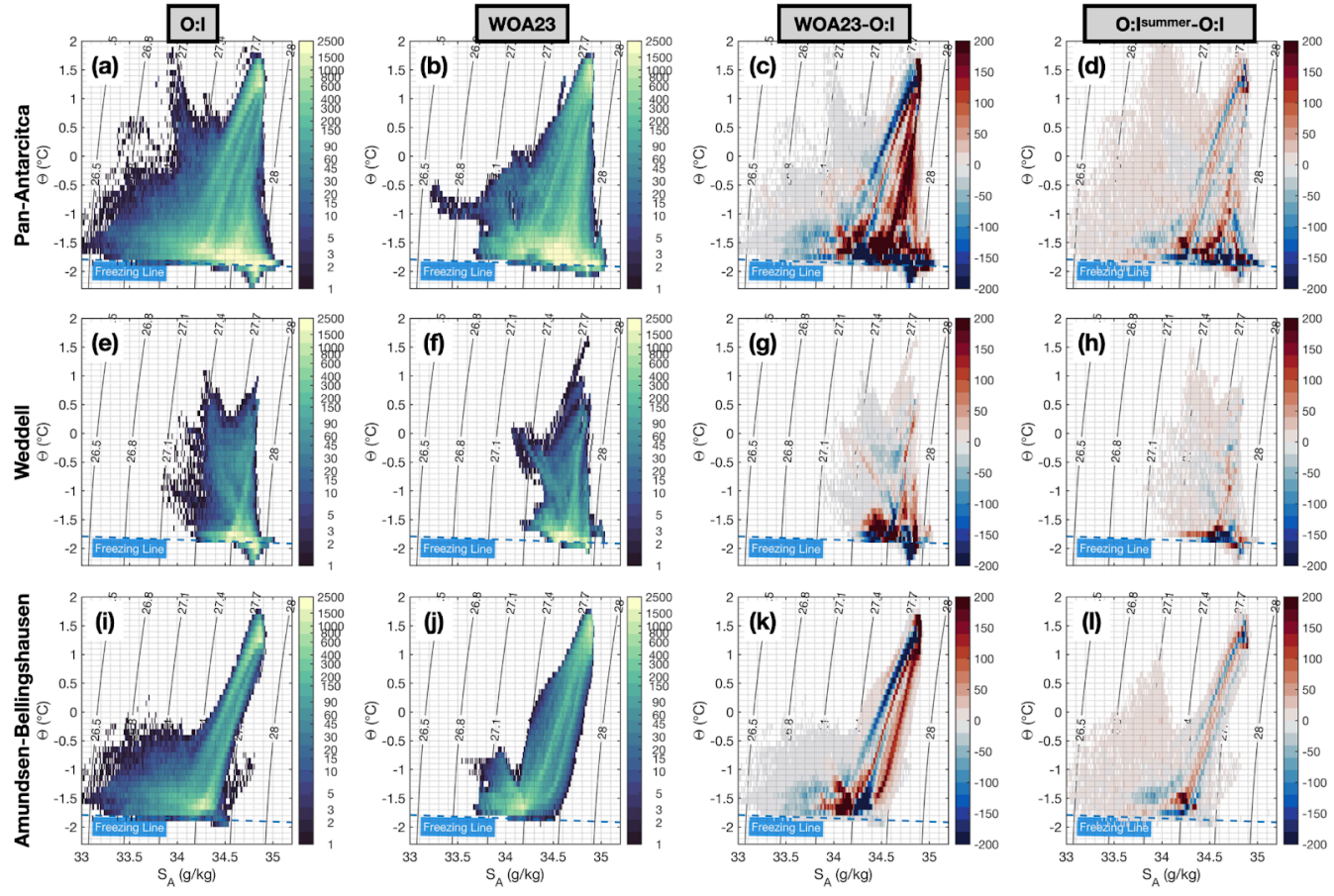

Figure 11. Probability Distribution Function (PDF) derived from the OCEAN ICE and WOA23 climatologies and their differences and the differences in PDF between OCEAN ICE summer climatology and the OCEAN ICE climatology in: a - d pan-Antarctic shelf seas; e-h Weddell Sea (60°W-15°E); i - l Amundsen-Bellingshausen Sea (150°W - 70°W).

Another artefact produced by coarser WOA23 interpolation and already mentioned earlier along vertical sections is revealed as a straight line in the T-S space connects two source water types - CDW and WW - in the Amundsen-Bellingshausen Sea (light red stripe in Fig. 11k), whilst the coarser bathymetry used in WOA23 also allows larger volumes of saltier waters available offshore to artificially flood the near-seabed continental shelf (large red stripe in Fig. 11k), a feature that is not actually observed (see also Fig. 10h, 10f). Closer to the surface, the O:I climatology captures the presence of a larger volume of a third source core water that is warmer and fresher: the summer/spring Antarctic surface water (e.g., Thompson et al. 2020, blue stripe in Fig. 11k). The regional differences between the two climatology products in the T-S space are imprinted to the pan-Antarctic comparison (Fig. 11c).

https://doi.org/10.5194/essd-2025-727
Preprint. Discussion started: 16 January 2026

5 Summary

In this paper, we present an updated hydrography profiles compilation. We provide an overview of the spatio-temporal distribution of the available data and a new metric to evaluate the ability of the profiles compilation in resolving temporal variability at different timescales over different regions. Three newly-developed O:I climatology products using the profiles compilation with a primary focus in the subpolar regions in the Southern Ocean and Antarctic continental shelf are created, and two are briefly presented. The O:I climatology design considers the dynamic connectivity between data points by constraining an anisotropic interpolation scheme using assimilated SSH product and incorporates the distinct dynamic regimes difference between open oceans and shelf seas by adjusting the interpolation radii of influence using bathymetry. The O:I climatologies are constructed such that the small lateral gradient of water mass distribution on the Antarctic continental shelf are resolved, in contrast to previous, more globally focused climatological products. The O:I climatologies can readily be used as a better initial/boundary condition for numerical models, or in evaluation exercises. The accurate representation of the thermal forcing of the shelf water masses is in particular critical for the ice sheet modelling community to derive a modern-day melting condition for future projection (e.g., Jourdain et al. 2020, Finucane and Stewart 2024). This compilation building exercise highlighted a need to combine various and sometimes disparate and not fully interconnected data sources. This is perhaps due to the somewhat irregular sampling nature of polar regions. We recognize large efforts are concentrating on aggregating profiles from all sources (e.g. WOA23) and hope gaps will be resolved soon. We aim to maintain this circum-Antarctic profile compilation in the future and would be happy to receive profile contributions from collaborators.

6 Data Availability

OCEAN ICE hydrography profiles compilation is available at https://doi.org/10.17882/99787 (Zhou et al. 2025a, last access: 28 September 2025). The O:I full, summer and 21st century climatologies are available at https://doi.org/10.17882/103946 (Zhou et al. 2025b, last access: 28 September 2025). Both dataset are in NetCDF format with intuitive description of variables, the key ones among which are mentioned in this data release paper.

Acknowledgement

This research was supported by Ocean Cryosphere Exchanges in ANtarctica: Impacts on Climate and the Earth system, OCEAN ICE, which is funded by the European Union, Horizon Europe Funding Programme for research and innovation under grant agreement Nr. 101060452, 10.3030/101060452. OCEAN ICE contribution number 18. This work was funded by UK Research and Innovation (UKRI) under the UK government's Horizon Europe funding Guarantee [grant number 0048443]. Authors would like to thank all the scientists, project principle investigators and ship crew members who are involved in collecting CTD profiles, Argo float deployments and seal taggings. This profiles compilation and climatology

https://doi.org/10.5194/essd-2025-727
Preprint. Discussion started: 16 January 2026

would not be possible without all these hard efforts of *in-situ* data acquisition. Shenjie Zhou, Pierre Dutrieux, Andrew Meijers, Tore Hattermann and Makus Janout received funding from OCEAN ICE. Claudia Giulivi was funded by NASA project 19-MAP19-0011 Assessing the Impact of Glacial Melt on the Coupled Climate (grant # 80NSSC20K1158). Tae-Wan Kim was supported by the Korea Polar Research Institute (KOPRI) grant funded by the Ministry of Oceans and Fisheries (grant no. PE25110). Won Sang Lee was supported by the Korea Institute of Marine Science & Technology Promotion (KIMST) funded by the Ministry of Oceans and Fisheries (RS-2023-00256677).

Author contribution

S. Z. and P. D jointly conceived the study. S. Z. curated the profile compilation, developed methodology and performed the climatology construction. P. D., C. G. helped gather raw profile data. W. L., T.-W. K., T. H. provided dataset that were not yet archived in public databases. P. D., A. M. and M. J. involved in the discussion of the methodology development and results interpretation. All authors contribute to revising this manuscript.

Competing interests

The authors declare that they have no conflict of interest.

Reference

1. Akhoudas, C.H., Sallée, J.B., Reverdin, G., Haumann, F. A., Pauthenet, E., Chapman, C. C., Margirier, F., Monaco, C. L., Metzl, N., Meilland, J. and Stranne, C.: Isotopic evidence for an intensified hydrological cycle in the Indian sector of the Southern Ocean. *Nat. Commun.*, 14, 2763. https://doi.org/10.1038/s41467-023-38425-5, 2023.
2. Barker, P. M and McDougall, T. J.: Stabilizing Hydrographic Profiles with Minimal Change to the Water Masses. *J. Atmos. Oceanic Technol.*, 34, 1935 - 1945. https://doi.org/10.1175/JTECH-D-16-0111.1, 2017.
3. Boyer, T., Levitus, S., Garcia, H., Locarnini, R. A., Stephens, C. and Antonov, J.: Objective analyses of annual, seasonal, and monthly temperature and salinity for the World Ocean on a 0.25° grid. *Int. J. Climatol.*, 25, 931 - 945. https://doi.org/10.1002/joc.1173, 2005.
4. Chu, P. C., and Fan, C. W.: A conserved minimal adjustment scheme for stabilization of hydrographic profiles. *J. Atmos. Oceanic Technol.*, 27, 1072–1083. https://doi.org/10.1175/2010JTECHO742.1, 2010.
5. Finucane, G., and Stewart, A. L.: A predictive theory for heat transport into iceshelf cavities. *Geophys. Res. Lett.*, 51, e2024GL108196. https://doi.org/10.1029/2024GL108196, 2024.

https://doi.org/10.5194/essd-2025-727
Preprint. Discussion started: 16 January 2026

6. Frölicher, T. L., Jorge L. Sarmiento, David J. Paynter, John P. Dunne, John P. Krasting and Winton. M.: Dominance of the Southern Ocean in Anthropogenic Carbon and Heat Uptake in CMIP5 Models. *J. Clim.*, 28(2), 862 - 886. https://doi.org/10.1175/JCLI-D-14-00117.1, 2015.
7. Garcia, H. E., Boyer, T. P., Locarnini, R. A., Baranova, O. K. and Zweng, M. M.: World Ocean Database 2018: User's Manual (prerelease). A.V. Mishonov, Technical Ed., NOAA, Silver Spring, MD. https://https://www.ncei.noaa.gov/sites/default/files/2020-04/wodreadme_0.pdf, 2018. (last access: 12 November 2025).
8. The IMBIE team: Mass balance of the Antarctic Ice Sheet from 1992 to 2017. *Nature*, 558, 219 - 222. https://doi.org/10.1038/s41586-018-0179-y, 2018.
9. Jackett, D. J., and McDougall, T. J.: Minimal adjustment of hydrographic profiles to achieve static stability. *J. Atmos. Oceanic Technol.*, 12, 381–389, https://doi.org/10.1175/1520-0426(1995)012%3C0381:MAOHPT%3E2.0.CO;2, 1995.
10. Janout, M. A., Hellmer, H. H.,Hattermann, T., Huhn, O., Sültenfuss, J., Østerhus, S., Stulic, L., Ryan, S., Schröder, M. and Kanzow, T.: FRIS revisited in 2018: On the circulation and water masses at the Filchner and Ronneice shelves in the southern Weddell Sea. *J. Geophys. Res. Oceans*, 126, e2021JC017269. https://doi.org/10.1029/2021JC017269, 2021.
11. Jenkins, A., Shoosmith, D., Dutrieux, P. et al.: West Antarctic Ice Sheet retreat in the Amundsen Sea driven by decadal oceanic variability. *Nat. Geosci.*, 11, 733 - 738. https://doi.org/10.1038/s41561-018-0207-4, 2018.
12. Johnson, G. C. and S. G. Purkey: Refined estimates of global ocean deep and abyssal decadal warming trends. *Geophys. Res. Lett.*, 51, e2024GL111229. https://doi.org/10.1029/2024GL111229, 2024.
13. Johnson, G. C., Lyman, J. M., Boyer, T., Cheng, L., Giglio, D., Gilson, J., Ishii, M., Killick, R. E., Kuusela, M., Locarnini, R., Mishonov, A., Oe, M., Purkey, S. G., Reagan, J., Sato, K. and Sukianto, T.: Ocean heat content. In state of the climate in 2023, global oceans. *BAMS*, 105(8), S173–S177. https://doi.org/10.1175/BAMS-D-24-0100.1, 2024.
14. Jourdain, N. C., Asay-Davis, X., Hattermann, T., Straneo, F., Seroussi, H., Little, C. M., and Nowicki, S.: A protocol for calculating basal melt rates in the ISMIP6 Antarctic ice sheet projections, *The Cryosphere*, 14, 3111 - 3134, https://doi.org/10.5194/tc-14-3111-2020, 2020.
15. Kim, Y. S. and Orsi, A. H.: On the Variability of Antarctic Circumpolar Current Fronts Inferred from 1992–2011 Altimetry, *J. Phys. Oceanogr.*, 44, 3054 - 3071. https://doi.org/10.1175/JPO-D-13-0217.1, 2014.
16. Kimura, S., Jenkins, A., Regan, H., Holland, P. R., Assmann, K. M., Whitt, D. B., Van Wessem, M., van de Berg, W. J., Reijmer, C. H. and Dutrieux, P.: Oceanographic controls on the variability of ice-shelf basal melting and circulation of glacial meltwater in the Amundsen Sea Embayment, Antarctica. *J. Geophys. Res. Oceans*, 122, 10131–10155. https://doi.org/10.1002/2017JC012926, 2017.

https://doi.org/10.5194/essd-2025-727
Preprint. Discussion started: 16 January 2026

17. Locarnini, R. A., A. V. Mishonov, J. I. Antonov, T. P. Boyer, H. E. Garcia, O. K. Baranova, M. M. Zweng, C. R. Paver, J. R. Reagan, D. R. Johnson, M. Hamilton, D. Seidov, 2013. World Ocean Atlas 2013, Volume 1: Temperature. S. Levitus, Ed.; A. Mishonov, Technical Ed.; NOAA Atlas NESDIS 73, 40 pp. https://www.ncei.noaa.gov/data/oceans/woa/WOA13/DOC/woa13_vol1.pdf. (last access: 12 November, 2025).
18. Lynn, R. G., and Reid J. L.: Characteristics and circulation of deep and abyssal waters. Deep-Sea Res., 15 , 577–598, https://doi.org/10.1016/0011-7471(68)90064-8, 1968.
19. Mazloff, M., P. Heimbach, and C. Wunsch: An Eddy-Permitting Southern Ocean State Estimate. *J. Phys. Oceanogr.*, 40, 880 - 899. https:/doi.org/10.1175/2009JPO4236.1, 2010.
20. McDougall, T. J. and P. M. Barker: Getting started with TEOS-10 and Gibbs Seawater (GSW) Oceanographic Toolbox, 28pp, SCOR/IAPSO WG127, ISBN 978-0-646-55621-5.
21. Nicholls, K. W., Østerhus, S., Makinson, K., Gammelsrød, T. & Fahrbach, E.: Ice-ocean processes over the continental shelf of the southern Weddell Sea, Antarctica: a review. *Rev. Geophys.*, 47, RG3003. https://doi.org/10.1029/2007RG000250, 2009.
22. Orsi, A. H. and Whitworth, T.: Hydrographic Atlas of the World Ocean Circulation Experiment (WOCE) Volume 1: Southern Ocean. https://doi.org/10.21976/C6BC78, 2005.
23. Purkey, S. G. and G. C. Johnson: Warming of Global Abyssal and Deep Southern Ocean Waters between the 1990s and 2000s: Contributions to Global Heat and Sea Level Rise Budgets. *J. Clim.*, 23(23), 6336 - 5351. https://doi.org/10.1175/2010JCLI3682.1, 2010.
24. Purkey, S. G. and G. C. Johnson: Global Contraction of Antarctic Bottom Water between the 1980s and 2000s. *J. Clim.*, 23(17), 5830 - 5844. https://doi.org/10.1175/JCLI-D-11-00612.1, 2012.
25. Purkey, S. G. and G. C. Johnson: Antarctic Bottom Water Warming and Freshening: Contributions to Sea Level Rise, Ocean Freshwater Budgets, and Global Heat Gain. *J. Clim.*, 26(16), 6105 - 6122. https://doi.org/10.1175/JCLI-D-12-00834.1, 2013.
26. Reagan, J.R., H.E. Garcia, T.P. Boyer, O.K. Baranova, C. Bouchard, S.L. Cross, D. Dukhovskoy, A. Grodsky, R.A. Locarnini, A.V. Mishonov, C.R. Paver, D. Seidov, and Z. Wang: World Ocean Atlas 2023: Product Documentation. A. Mishonov, Technical Editor, https:/doi.org/10.25923/a78k-gq49, 2023.
27. Ridgway, K. R., Dunn, J. R. and Wilkin, J. L.: Ocean Interpolation by Four-Dimensional Weighted Least Squares - Application to the Waters around Australasia, *J. Atmos. Oceanic Technol.*, 19, 1357 - 1375. https://doi.org/10.1175/1520-0426(2002)019<1357:OIBFDW>2.0.CO;2, 2002.
28. Roquet F., Guinet C., Charrassin J.-B., Costa D. P., Kovacs K. M., Lydersen C., Bornemann H., Bester M. N., Muelbert M. C., Hindell M. A., McMahon C. R., Harcourt R., Boehme L., Fedak M. A., Doriot V., Picard B.: MEOP-CTD in-situ data collection: a Southern ocean Marine-mammals calibrated sea water temperatures and salinities observations. SEANOE. https://doi.org/10.17882/45461, 2024.

https://doi.org/10.5194/essd-2025-727
Preprint. Discussion started: 16 January 2026

29. Sallée J. B., Abrahamsen E. P., Allaigre C., Auger M., Ayres H., Badhe, R., Boutin, J., Brearley, J. A., de Lavergne, C., ten Doeschate, A. M. M., Droste, E. S., du Plessis, M. D., Ferreira, D., Giddy, I. S., Gülk, B., Gruber, N., Hague, M., Hoppema, M., Josey, S. A., Kanzow, T., Kimmritz, M., Lindeman, M. R., Llanillo, P. J., Lucas, N. S., Madec, G., Marshall, D. P., Meijers, A. J. S., Meredith, M. P., Mohrmann, M., Monteiro, P. M. S., Mosneron Dupin, C., Naeck, K., Narayanan, A., Naveira Garabato, A. C., Nicholson, S-A., Novellino, A., Ödalen, M., Østerhus, S., Park, W., Patmore, R. D., Piedagnel, E., Roquet, F., Rosenthal, H. S., Roy, T., Saurabh, R., Silvy, Y., Spira, T., Steiger, N., Styles, A. F., Swart, S., Vogt, L., Ward, B. and S. Zhou, S.: Southern ocean carbon and heat impact on climate. *Phil. Trans. R. Soc. A.*, 38120220056. http://doi.org/10.1098/rsta.2022.0056, 2023.
30. Schaffer, J., Timmermann, R., Arndt, J. E., Kristensen, S. S., Mayer, C., Morlighem, M., and Steinhage, D.: A global, high-resolution data set of ice sheet topography, cavity geometry, and ocean bathymetry, *Earth Syst. Sci. Data*, 8, 543–557, https://doi.org/10.5194/essd-8-543-2016, 2016.
31. Schmidtko, S., G. C. Johnson, and J. M. Lyman: MIMOC: A global monthly isopycnal upper-ocean climatology with mixed layers, *J. Geophys. Res. Oceans*, 118, 1658–1672, https://doi.org/10.1002/jgrc.20122, 2013.
32. Schmidtko, S., K. J. Heywood, A. F. Thompson, and S. Aoki: Multidecadal warming of Antarctic waters. *Science*, 346, 1227 - 1231, https://doi.org/10.1126/science.1256117, 2014.
33. Siedler, G., Church, J., and Gould, J. (Eds.): Ocean Circulation and Climate: Observing and Modelling the Global Ocean, Academic Press, London, 715 pp., ISBN 978-0-12-026143-1, 2001.
34. Tamura, T., K. I. Ohshima, A. D. Fraser,and G. D. Williams: Sea ice production variability in Antarctic coastal polynyas. *J. Geophys. Res. Oceans*, 121, 2967 - 2979. https://doi.org/10.1002/2015JC011537, 2016.
35. Tamsitt, V., Drake, H.F., Morrison, A.K., Talley, L. D., Dufour, C. O., Gray, A. R., Griffies, S. M., Mazloff, M. R., Sarmiento, J. L., Wang, J. and Weijer, W.: Spiraling pathways of global deep waters to the surface of the Southern Ocean. Nat Commun 8, 172. https://doi.org/10.1038/s41467-017-00197-0, 2017.
36. Thompson, A. F., Speer, K. G. and Schulze Chretien, L. M.: Genesis of the Antarctic Slope Current in West Antarctica. *Geophys. Res. Lett.*, 47, e2020GL087802. https://doi.org/10.1029/2020GL087802, 2020.
37. Walker, D. P., A. Jenkins, K. M. Assmann, D. R. Shoosmith, and M. A. Brandon: Oceanographic observations at the shelf break of the Amundsen Sea, Antarctica, *J. Geophys. Res. Oceans*, 118, 2906–2918. https://doi.org/10.1002/jgrc.20212, 2013.
38. Wang, X., Chu, P. C., Han, G., Li, W., Zhang, X. and Li, D.: A Fully Conserved Minimal Adjustment Scheme with (T, S) Coherency for Stabilization of Hydrographic Profiles. *J. Atmos. Oceanic Technol.*, 29, 1854–1865. https://doi.org/10.1175/JTECH-D-12-00025.1, 2012.
39. Williams, R.G., Meijers, A.J.S., Roussenov, V.M., Katavouta, A., Ceppi, P., Rosser, J. P. and Salvi, P.: Asymmetries in the Southern Ocean contribution to global heat and carbon uptake. *Nat. Clim. Chang.*, 14, 823 - 831. https://doi.org/10.1038/s41558-024-02066-3, 2024.

https://doi.org/10.5194/essd-2025-727
Preprint. Discussion started: 16 January 2026

635 40. Yamazaki, K., Aoki, S., Shimada, K., Kobayashi, T. and Kitade, Y.: Structure of the subpolar gyre in the
636 Australian-Antarctic Basin derived from Argo floats. *J. Geophys. Res. Oceans*, 125, e2019JC015406.
637 https://doi.org/10.1029/2019JC015406, (2020).
638 41. Yamazaki, K., Bindoff, N. L., Phillips, H.E., Nikurashin, M., Herraiz-Borreguero, L., and Spence, P.: Unlocking
639 Southern Ocean under-ice seasonality with a new monthly climatology. *J. Geophys. Res. Oceans*, 130,
640 e2024JC020920. https://doi.org/10.1029/2024JC020920, (2025).
641 42. Yang, H. W., Kim, T. W., Dutrieux, P., Wåhlin, A. K., Jenkins, A., Ha, H. K. ,Kim, C. S., Cho, K.-H., Park, T., Lee,
642 S. H. and Cho Y.-K.: Seasonal variability of ocean circulation near the Dotson Ice Shelf, Antarctica. *Nat. Commun.*,
643 13, 1138, https://doi.org/10.1038/s41467-022-28751-5, 2022.
644 43. Zhou, S., Meijers, A. J. S., Meredith, M. P., Abrahamson, E. P., Holland, P. R., Silvano, A., Sallée, J.-B. and
645 Østerhus, S.: Slowdown of Antarctic Bottom Water export driven by climatic wind and sea-ice changes. *Nat. Clim.*
646 *Chang.*, 13(7), 701–709. https://doi.org/10.1038/s41558-023-01695-4, 2023.
647 44. Zhou, S., Dutrieux, P., Giulivi, C., Lee, W., Kim, T.-W., Hattermann, T. and Janout, M.: Southern Ocean
648 (90°S-45°S) conservative temperature and absolute salinity profiles compilation (OCEAN ICE D1.1). SEANOE
649 [dataset], https://doi.org/10.17882/99787, 2025a.
650 45. Zhou, S., Dutrieux, P. and Giulivi, C.: The OCEAN ICE Southern Ocean Climatology. SEANOE [dataset],
651 https://doi.org/10.17882/103946, 2025b.
652